
Volume 1 | Number 1 | Jan 2013 | Pages 1–100
RSC Advances
www.rsc.org/advances
ROYAL SOCIETY OF CHEMISTRY

Conductive nanocomposite hydrogels with self-healing property

Rengui Peng, Yang Yu, Sheng Chen, Yingkui Yang, Youhong Tang

Graphical abstract

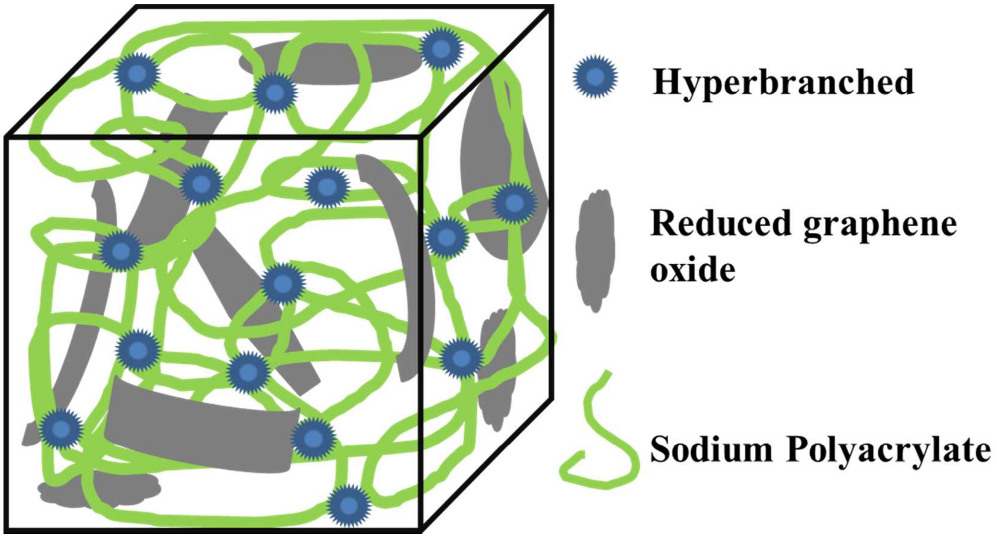

Conductive nanocomposite hydrogels with self-healing property

Rengui Peng [1, #], Yang Yu [1, #], Sheng Chen [2], Yingkui Yang [3], Youhong Tang [1, *]

[1] Centre for NanoScale Science and Technology and School of Computer Science, Engineering and Mathematics, Flinders University, South Australia 5042, Australia

[2] School of Chemical Engineering, The University of Adelaide, South Australia 5005, Australia

[3] Key Laboratory for Green Preparation & Application of Functional Materials, Ministry of Education, and Faculty of Materials Science & Engineering, Hubei University, Wuhan 430062, China

[#] Equal contribution

* Corresponding author: Tel.: 61-8-82012138. E-mail: youhong.tang@flinders.edu.au (Y Tang)

Abstract

A flexible, electrically conducting hydrogel with self-healing repeatability can be of use in emerging fields such as soft passive resistors/capacitors and electro-active soft sensor devices, but combining all these properties remains a challenging task. Here, we report a versatile hydrogel composite produced from commercial superabsorbent polymer and hyperbranched polymer with reduced graphene oxide (rGO) by a simple fabrication method. The composites show excellent electrical self-healing properties (completely healed after 20 seconds) with ultra-high water-absorption ability up to 350 times normal in ambient condition. The composites possess excellent water-absorption reusability and the water-absorption ability can be adjusted by changing the amounts of rGO and hyperbranched polymer in the composites. The electrical conductivity can also be modified by varying the amount of absorbed water, and the product would be a good candidate for soft moisture-related resistors/sensor systems.

Keywords

Nanocomposite hydrogel, self-healing, conductivity, superabsorbent

1. Introduction

As aggregations of polymer networks and water, hydrogels are abundant in natural and man-made materials. Owing to their unique solid and liquid properties, hydrogels have been extensively explored and are widely used in diverse applications such as absorbents in waste management, media for electrophoresis, coatings for medical devices, packers in oilfield and sensors and actuators in soft machines.[1-3] As a combination of solid and liquid components, gels differ from conventional solids in their mechanical properties and in their response to external stimuli. In particular, gels can undergo large changes in volume by exuding or absorbing water, and this in turn leads to changes in most other properties.[1]

As a new class of polymer hydrogels, superabsorbent polymer (SAP) materials were discovered and reported first by the U.S. Department of Agriculture.[4] They are three-dimensional, cross-linked and hydrophilic networks of polymer chains, which can absorb and retain a large amount of water or other aqueous solutions, even under some pressure, in comparison with their own mass.[5, 6] SAPs can be classified as hydrogels with ultra-high water-absorption ability (1,000 - 100,000 %), whereas common hydrogels lack the ability to absorb a large amount of water (~100 %).[7] Due to their low cost, high hydrophilicity, low toxicity and biocompatibility, SAPs can be applied in areas where high absorption is needed. In the last decade, to enhance their absorption capacity and adapt them for certain applications, SAPs have been filled with natural and synthesized fillers, and the product is then called a SAP composite.[8-10]

Most traditional hydrogels have certain disadvantages such as brittleness, low swelling ability, non-conductivity, lack of self-healing ability, and poor mechanical strength and transparency.[6, 11, 12] Remarkable improvements have been made to improve the hydrogel structures, such as topological (TP) gels,[13, 14] double-network (DN) gels[15, 16] and nanocomposite polymer (NC) gels [17-19], using different approaches. TP gels have figure-of-eight cross-linkers that can slide along the polymer chains. Reflecting this flexible cross-linkage, TP gels absorb large amounts of water and can be highly stretched without fracture. In NC gels, polymer chains are cross-linked by inorganic nano-slabs (clay is the focus of current researches) on the scale of a several tens of nanometers, instead of organic cross-linking agents. NC gels are also highly stretchable and possess other favourable physical properties such as excellent optical transparency. Finally, DN gels consist of two interpenetrating polymer networks: one is made of highly cross-linked rigid polymers and the other of loosely cross-linked flexible polymers. The invention of these three novel gel types has not only achieved a breakthrough in introducing wide application of gels to industry and biomedical fields; it has also posed fundamental problems in gel science. An important advantage of NC gels is their simplicity of synthesis. It is easy to induce new structure to NC gels by modifying the technique. Nanotechnologies offer opportunities to develop complex and optimized soft materials with synergistic properties. The possibility of controlling chemical and physical properties via the design of 3D gel structures provides a powerful strategy for incorporation of versatility into engineering gels from the nanometer scale. For example, Aida *et al.* used sodium polyacrylate (ASAP), clay nanosheets (CNSs) and dendritic macromolecule Gn-binder to fabricate free-standing mouldable hydrogels with great mechanical strength and self-healing capability.[20] The ASAP-wrapped CNSs were cross-linked with Gn-binder by non-covalent forces which facilitated the rapid self-healing ability of the material.[20] Bao *et al.* described a method to develop a supramolecular organic polymer composite embedded with nickel nanostructured micro-particles, which had mechanical and electrical self-healing properties.[21] The conductivity of the composite was repeatedly restored with ~90% efficiency after 15 s, and the mechanical properties were completely restored after ~10 min.

Meanwhile, the electronic properties of SAPs could be potentially enhanced by incorporating other conductive nanoparticles/nanosheets. A good candidate for this is graphene, a single layer of graphite nanosheet arranged in a honeycomb lattice form with unique electronic, mechanic and thermal properties.[22] Due to the high-cost of graphene production (e.g. mechanical cleaving, sonication and surfactant-assisted exfoliation), reduced graphene oxide (rGO) with comparable electronic properties is considered a suitable alternative to graphene that can be produced by the low-cost chemical reduction of graphene oxide (GO).[22, 23] In this study, we have prepared a versatile hydrogel material by combining commercial SAP with rGO to achieve superior water absorbency, high conductivity and excellent electrical self-healing ability through a simple fabrication method.

2. Experimental

Sodium polyacrylate polymer particles (superabsorbent polymer; SAP) and hyperbranched bis-MPA polyester-64-hydroxyl (HB) were purchased from Sigma-Aldrich. Reduced graphene oxide (rGO) was prepared by oxidizing graphite powder following the modified Hummers method and exfoliation of their suspensions under bath ultrasonication.[24-26] Then 7.5 mg of the rGO powder was dispersed in 50 mL Milli-Q water under bath ultrasonication for 1 h to obtain a stable suspension. 260 mg SAP and 78 mg HB were then added into the rGO suspension and mixed thoroughly. This mixture was poured into a Teflon-lined stainless steel autoclave and heated at 100℃ for 10 h, forming a conductive, self-standing material. The proportion of SAP: rGO: binder was 10: 0.25: 3, which was denoted as SRB0.25. By varying the amount of rGO used in the mixture, different rGO/SAP samples were prepared, such as SRB0.50, SRB1.00 and SRB1.50.

Transmission electron microscopy (TEM) images of rGO were obtained using a transmission electron microscope (Philips CM200, the Netherlands) at 200 kV. For the preparation of the TEM specimens, rGO nanoparticles were dispersed in acetone and sonicated by an ultrasonication pin (SKL-950IIDN, Ningbo Haishu Sklon Electronic Instrument Ltd., China) for 5 min, and the solution was dropped onto carbon coated copper grids for TEM observation after the evaporation of the solvent. A Fourier transform infrared spectrometer (Nicolet iN10 MX FTIR Microscope, Thermo Scientific, US) was used in absorption mode. Spectral resolution of the FTIR was maintained at 2 cm^{-1}. The sample was made into a thin potassium bromide (KBr) pellet using dry KBr at a 1:100 ratio (sample : KBr). Raman spectroscopy is widely used as a non-destructive spectroscopic technique for the structural characterization of graphitic materials. Raman measurements of the SAP/HB (SB) and SRB samples were carried out on an Alpha300RS microscopy/spectroscopy instrument (Witec, Germany) using a 532 nm laser with a maximum power of <60 mW. Single spectra were recorded at an acquisition time of 10 s.

The strips of the composite sheets were weighed and immersed into ambient temperature DI water. The samples were removed at specified intervals, gently blotted with tissue paper to remove the excess water, and the weight of each swollen sample was recorded. This was repeated at several time intervals until the samples reached equilibrium state, after which they were dried to a constant weight. The degree of swelling by weight W_s in each sample was calculated by $W_s = \frac{W_2 - W_1}{W_1} \times 100\%$, where W_1 and W_2 are the weights of the sample before immersion in water and after swelling with water for a certain period, respectively.

Scanning electron microscopes (CAMScan MX2500 SEM, the Netherlands) were employed to study the fracture surfaces of the composite specimens. Composites with the water-absorption ratio of 100% were immersed in liquid nitrogen for 1 hr before being fractured inside the liquid nitrogen by forceps. The fractured samples were immediately placed in a freeze-dryer overnight before being sputter-coated with a 2 nm layer of Pt to minimize surface charging.

Resistivity measurements were performed using an Agilent 3440 Digital Multimeter. The sample was loaded between two parallel aluminium discs of 12.6 mm diameter. A controllable amount of DI water had been absorbed in the sample before characterization was conducted. At least 10 measurements were conducted for each data point.

3. Results and discussion

The TEM image shows that the rGO has a sheet-like structure with the lateral size of several micrometres (Fig. 1). The carbon sheet is very thin and is almost transparent to electron beams. The wrinkles across whole sheets signify the introduction of rich functional groups like epoxyl (-COC-), hydroxyl (-OH) and carboxyl (-COOH) groups,[27] also evidenced by the FTIR results in Fig. 2. On the one hand, these functional groups render the rGO hydrophilic in nature and compatible with a wide range of solvents for further processing. On the other hand, these functional groups might also act as anchor sites to interact with SAP polymer and HB polymer binder to generate the hybrid material. Fig. 2 shows the FTIR spectra curves of rGO, SB and SB1.00 hydrogel samples. For the rGO sample, the broad peak at 3411 cm^{-1} is attributed to the stretching vibrations of hydroxyl groups.[28] The peaks at 1050 cm^{-1} can be ascribed to C-O stretching.[29] The peak at 1576 cm^{-1} corresponding to C=C is attributed to the skeletal vibrations of graphitic domains from the basal plane of the rGO.[30] Compared with the rGO sample, SB has similar functional groups, including -OH, C=C and C-O (Fig. 2). A new peak appears at

1717 cm^{-1} in the FTIR spectra of SB and SB1.00 samples is attributed to carbonyl stretching vibration of SAP, indicating the formation of polyacrylate in those composites.[29, 31]

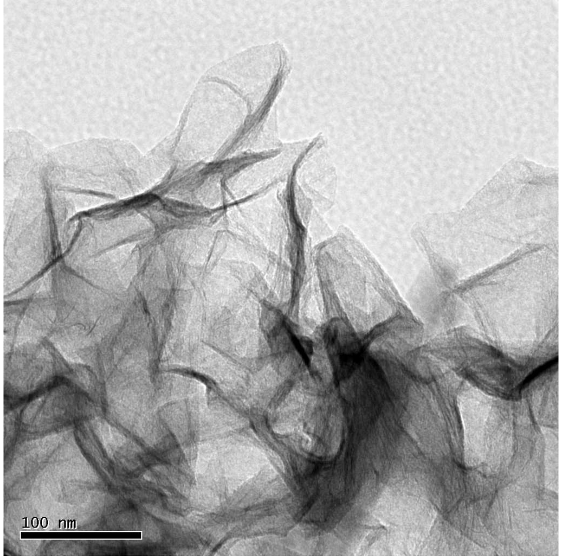

Fig. 1 Typical TEM image of reduced graphene oxide used.

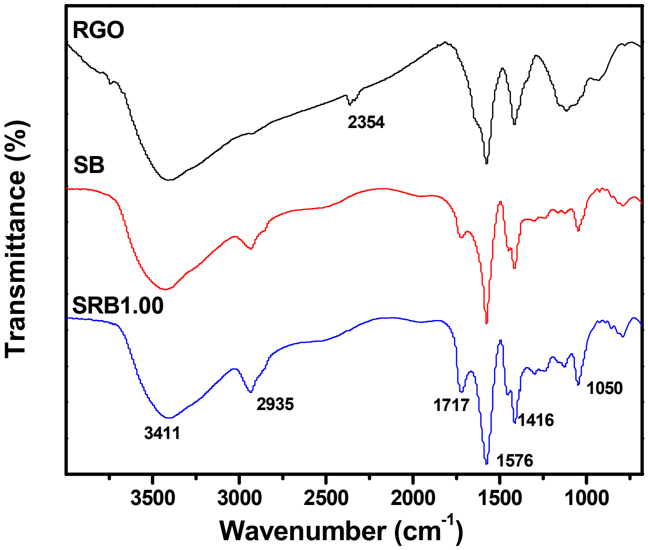

Fig. 2 FTIR spectra of rGO, SB and SRB1.00 with marked typical peaks.

Fig. 3 shows the Raman spectra of rGO, pure SB and SRB0.25 ~ SRB1.50 samples. For the rGO powder, two characteristic peaks at 1350 cm^{-1} and 1600 cm^{-1} are observed which can be attributed to the D-band and G-band, respectively.[28, 32] The relatively high intensity of the D-band in the rGO sample indicates the presence of numerous oxidative defects in the graphene lattice and demonstrates that the reduction process does not produce an rGO product with the same properties as pristine graphene.[22] Graphene has excellent conductivity, but the resistance of the rGO may be much higher than that of graphene due to the scattering of electrons on the nanosheets caused by remaining oxygen-containing groups and other functional groups introduced during the reduction.[33] On the other hand, oxygen-containing groups (e.g. hydroxyl, carboxyl and epoxy groups) on the rGO sample may form hydrogen bonding with the hydroxyl groups from the SAP polymer and HB polymer binder during the synthesis process, enhancing the dispersion and compatibility of the starting materials in the hydrogel’s network as well as the hydrophilicity of the prepared rGO/SAP composite hydrogels. In this case, partially reduced rGO was selected in this study owing to its high compatibility, hydrophilicity and relatively high conductivity. No Raman scattering was observed in the pure SB sample and two new peaks at 1350 cm^{-1} and 1600 cm^{-1} appear in the SRB samples (0.25 - 1.50) (Fig. 3). The intensity of the D-band and G-band of the SRB samples increased gradually with the higher composition of rGO, and the D/G intensity ratio was similar to that of the rGO sample, indicating the successful incorporation of rGO into the SAP structure.

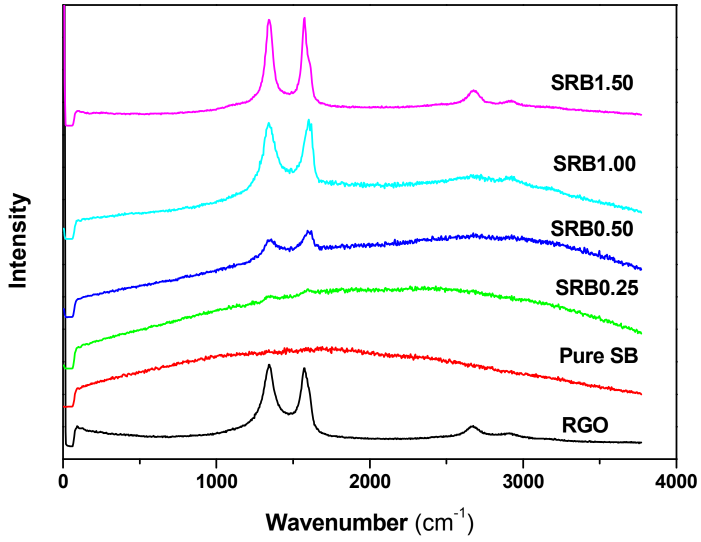

Fig. 3 Raman spectra of rGO, pure SB and SRB0.25-1.50 samples.

After immersion in Milli-Q water for 7 days, the rGO/SAP sample (SRB 1.00) was composed of 42869 % water and maintained its form and integrity without dissolving in water (Fig. 4). The rGO/SAP sample could be reused for water-absorption/desorption and the water absorbency remained the same after several water-absorption/desorption cycles (Fig. 4).

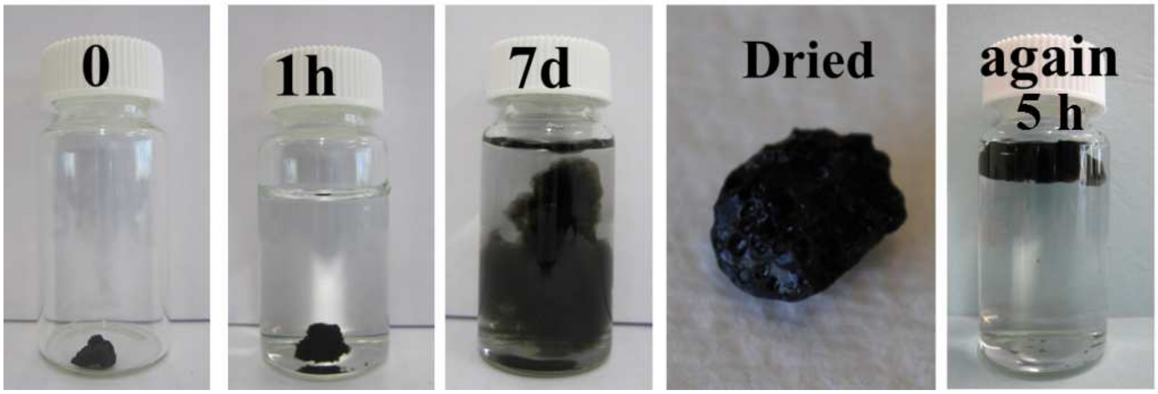

Fig. 4 Photo images of SRB1.00 sample at different water-absorption stages.

The rGO/SAP composite had very high extensibility, being able to withstand at least 5-times elongation and maintain the ability to restore its original conformation, as shown in Fig. 5. Fig. 6 illustrates possible interactions between different raw materials, which may physically entangle with each other in the composite matrix. The sodium polyacrylate polymer particles are a commercial product with various functional groups (e.g. -COOH, -OH, -COO$^-$) in the structure (as shown in Fig. 2) and the hyperbranched polymer binder is a hydroxyl group-rich dendrimer, which can interact with the sodium polyacrylate polymer particles and rGO through hydrogen bonding, enhancing the compatibility of the raw materials. It has highly stretchable properties, as reported by other researchers on NC gels.

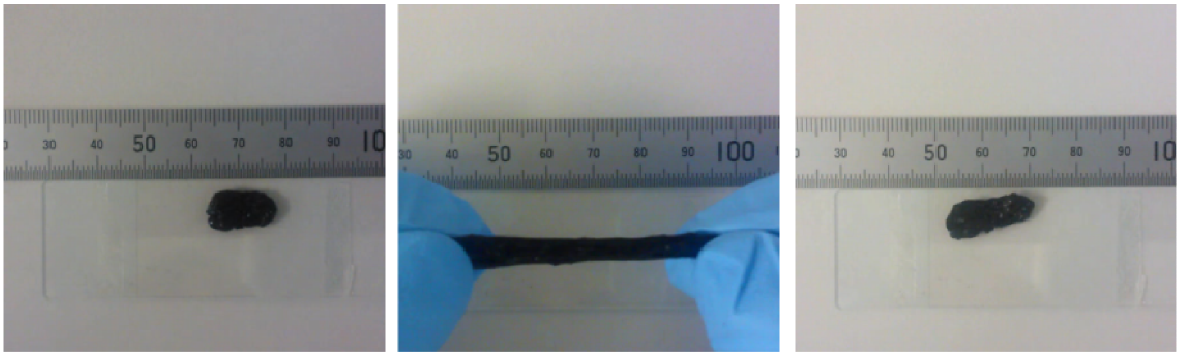

Fig. 5 Demonstrated high extensibility of SRB1.00 sample (Supplementary Movie 1).

The water-absorbing curves of composites are reported in Fig. 7. The plots of absorption ratio (W_s) vs. soak time are presented with two time zones (0 - 100 min and 100 - 570 min). In the first time zone (0 - 100 min), with an increase in soak time, the dramatic increase in absorption expedites the water-swelling properties of the composites. The SB composite has the highest water-swelling ability and reaches its maximum W_s of > 40K compares to its original weight. Composites of SB with rGO also can achieve around 18K - 35K % of original weight absorption abilities, depending on the rGO composition, as shown in Fig. 7(a). However, the slopes of W_s vs. soak time (water-absorption rate) have the different trend as the absorption ability of the composite at the initial stage, with SB having the lowest water-absorption rate, as shown in Fig. 7(b). With the addition of rGO in SB composites (SRB 0.25 - 1.50), the water-absorption abilities decreased but the initial absorption rate increased with the composites still possessed high water-absorption ability. In the second time zone (100 - 570 min), all the composite hydrogels maintained their maximum water-absorption capacities with slight variations, showing excellent water retention.

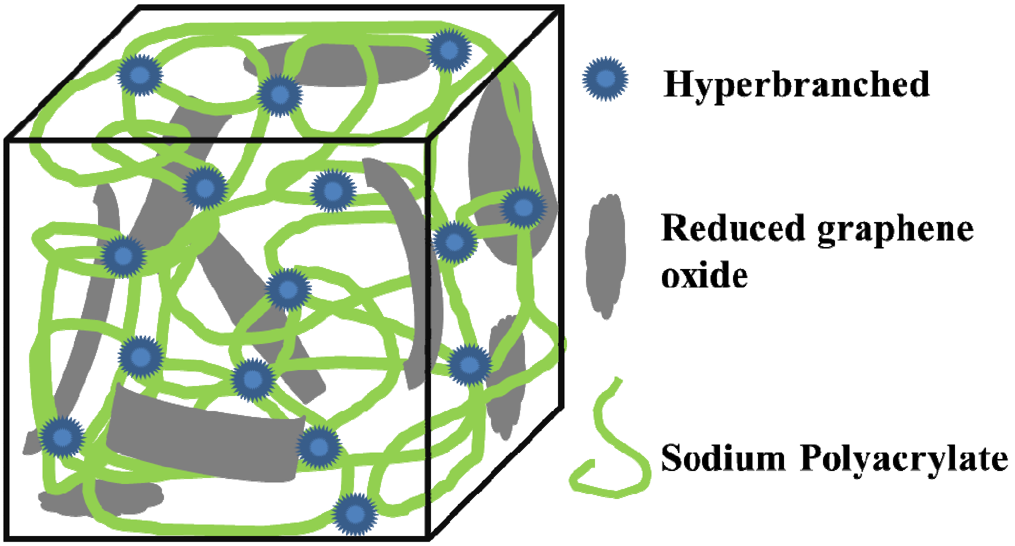

Fig. 6 Illustration of structure and interactions among the raw materials in the superabsorbent hydrogel.

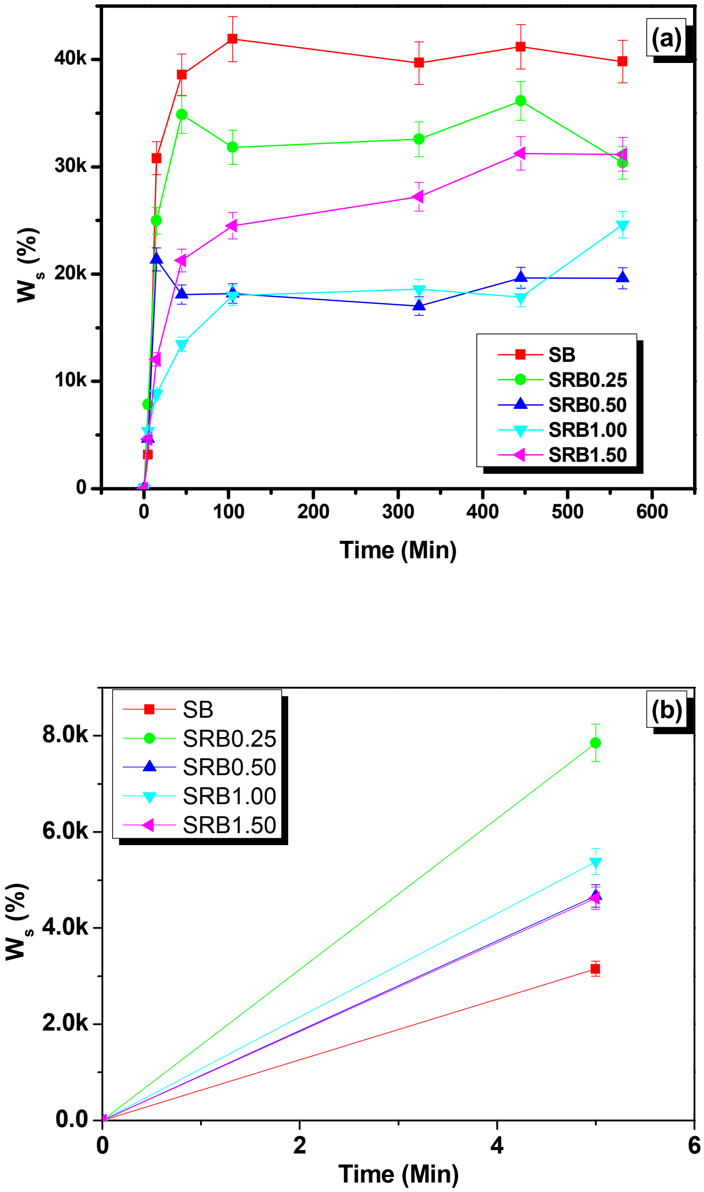

Fig. 7 Water-absorption ability and efficiency of SB and SRB samples at (a) reach steady state and (b) initial state.

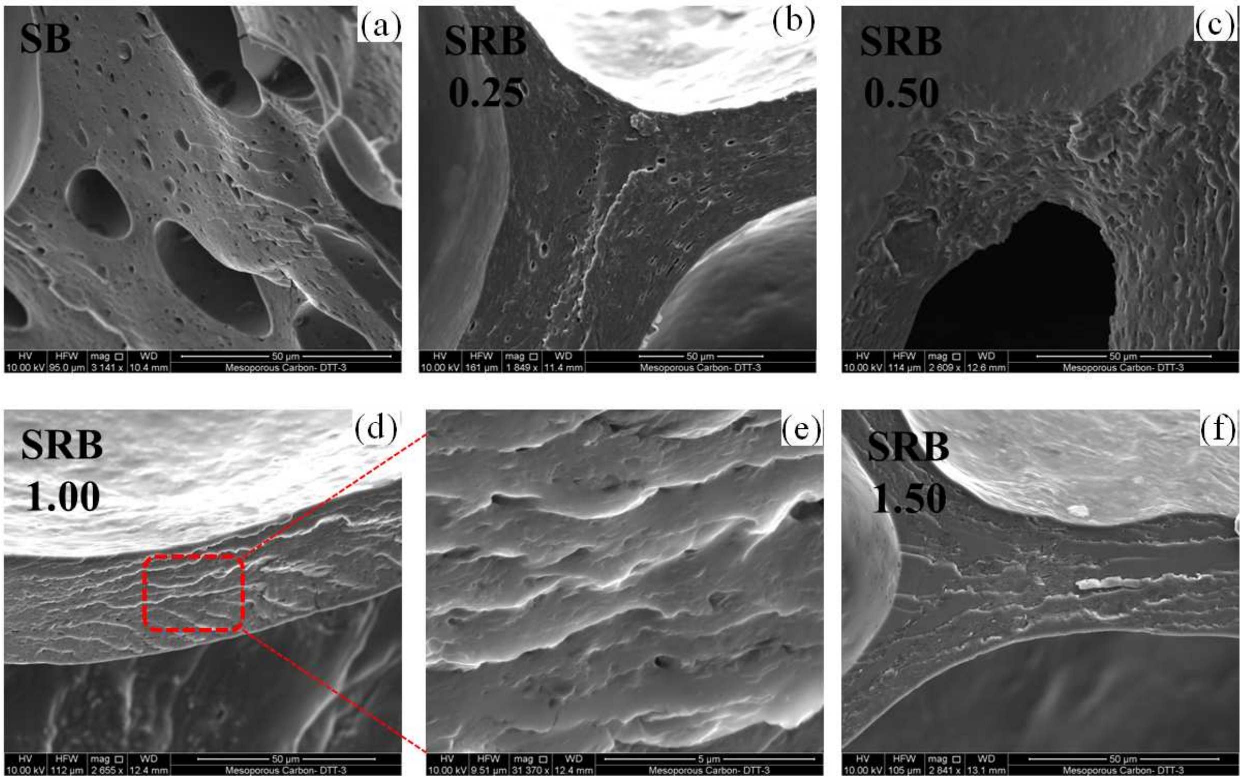

Fig. 8 Cross-sectional SEM images of freeze-dried SB and SRB samples.

Cross-sectional SEM images of freeze-dried SB and SRB samples, preserving the morphology of these samples well after water absorption, are shown in Fig. 8. From the SEM images, up to 1.5 % of the rGO are nanosheets were dispersed uniformly without aggregation in the SAP structure, indicating the compatibility and strong interfacial interactions of different raw materials at the interface. Various capillary tube structures can be observed in all samples, which may act as internal ‘water channels’ to connect the ‘water reservoirs’, as shown in Fig 8(e). This may be due to the presence of hydrophilic oxygen-containing groups on the rGO nanosheets enhancing water transportation and forming these tiny water channels. The internal ‘water channels’ increase the initial absorption rate of the composites, as shown in Fig. 7(b), however, the interactions between the raw materials (shown in Fig. 6) confine the swelling ability of SB and cause the disease of the final (steady state) absorption ability of SB. To further verify the dispersion of rGO nanosheets, the variation of resistance within each sample was measured (shown in Fig. 9). The resistance was found to be linear-proportional to the distance between two probes, indicating that the rGO nanosheets dispersed uniformly within the SAP network without any aggregations.

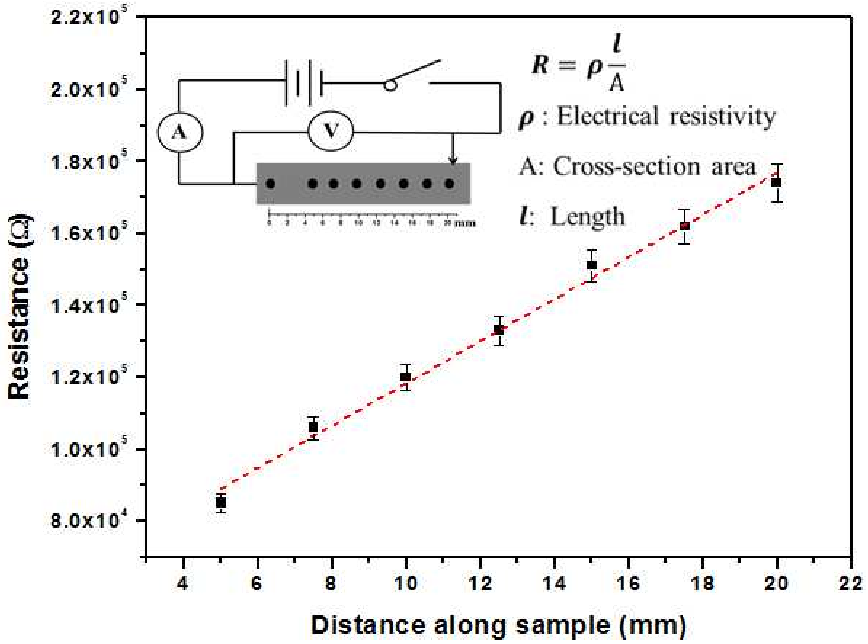

Fig. 9 Linear resistance variation across SRB1.00 sample.

Two parallel aluminium discs with a plastic restrainer around them were used to maintain the cylindrical shape of the sample and the resistivity of each sample was measured accordingly, as shown in Fig. 10. The average resistivity was plotted with standard deviation in Fig. 10 and the results show that the resistivity of different samples was remarkably influenced by water content. A completely dried SB sample was non-conducting, due to the absence of free electrons/ions in the SAP network. The dried SRB samples (SRB0.25-1.50) were also electrically non-conductive, because the small fraction of rGO nanosheets dispersed in the network without interconnecting in the non-conductive dried SB matrix could not make the whole composites conductive. The resistivity of all the samples decreased as a function of water content (e.g. $\sim 4\times10^{4}\Omega\cdot$M at 24 %) and reached a plateau ($\sim 1\times10^{3}\Omega\cdot$M) in the range of 270 % - 380 % water content. The results show that water content is the key factor that influences the resistivity of pure SB and SRB samples as well as transforming the material from non-conductive to conductive at different water contents. This is due to the fact that SB polymer is a sodium polyacrylate composite which releases free Na^+ cations into the solution of the polymer matrix with an increase in water content and decreases the resistivity of the polymer.[29] The Na^+ concentration decreases while the volume of the sample increases as a function of water content, and both influence the resistivity of the SAP sample to reach a minimum value at a certain level of water content (270 % - 380 %). In the range of 100 - 380 % water content, the rGO nanosheets enhance the conductivity of the SRB samples compared with that of the pure SB sample (Fig. 10(b)). This is due to the conductive rGO nanosheets acting as water channels connecting different water reservoirs and facilitating better water dispersion and more free ion (e.g. Na^+) transportation within the SAP networks than in the pure SB sample. For instance, pure SB had a minimum resistivity of 1.7×10^3 Ω·M whereas the resistivity of the rGO incorporated SRB sample was lower than 1.5×10^3 Ω·M (e.g. the resistivity of SRB 1.00 reached 267 Ω·M). The additional rGO in the SAP structure made the resistivity of SRB samples more sensitive to water content and the samples were thus more likely to become conductive.

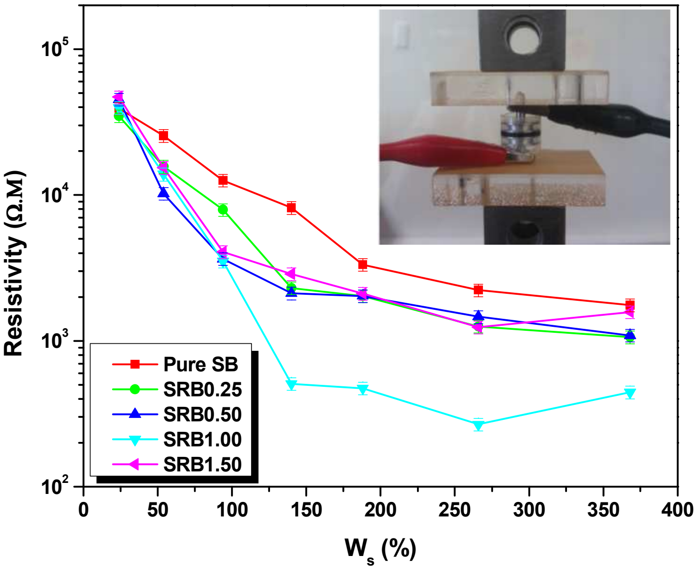

Fig. 10 Resistivity of SB and SRB samples as a function of water content with insertion in the resistivity test setup.

To demonstrate the electrical healing ability of the rGO/SAP composite, a battery-powered circuit with an SRB sample (SRB 1.00 with 140 % water content) connected to an illuminated light-emitting diode (LED) was fabricated (Fig. 11(a)). After the SRB sample was completely cut off, the circuit became open and the LED went off (Fig. 11(b)). Then the two fractured free-cut surfaces were brought together with gentle pressure for 20 s and the LED lit up again (Fig. 11(c)). Moreover, the composite became self-supporting and self-healing, as the two parts of the sample remained attached even when gently stretched (Fig. 11(d)). This was due to the re-association of the hydrogen bonds from the SAP polymer, rGO and hyperbranched polymer binder, which activated the high electrical healing efficiency of the material.[21] At the healing interface, the SAP polymer, rGO nanosheets and HB polymer binder were closely packed and bonded through the hydrogen bonds under gentle pressure.[21] Fig. 12 shows a time evolution of successive cutting–healing processes at the same position on an SRB 1.00 sample. An open circuit was formed following complete cut of the composite, at which point the resistance increased to 1×10^{39} Ω. As the two surfaces were brought into contact with gentle pressure for 30 s, the conductivity increased and the resistance reverted to its initial value (5×10^{4} Ω). The cutting–healing process was repeated 6 times at the same position and nearly full restoration of the electrical properties of the sample was observed. The hydrogen bonds from the SAP polymer, rGO and HB polymer binder activated the mechanical healing of the composite so that ions (e.g. Na^+) could transfer freely in the matrix.[21]

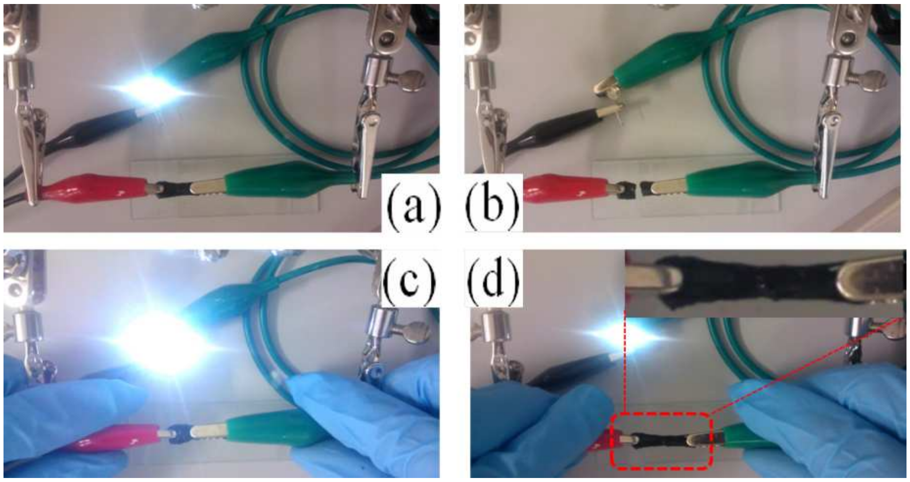

Fig. 11 Electrical healing efficiency of self-healing SRB1.00 sample. (a) pristine undamaged sample, (b) completely cut sample (open circuit), (c) contact and healing; (d) healed sample being stretched to show complete healing after 20 seconds at room temperature (Supplementary Movie 2)

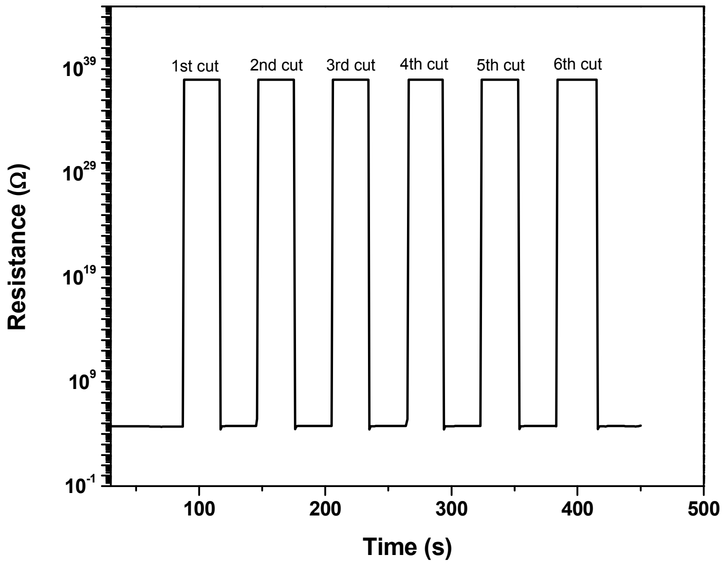

Fig. 12 Successive electrical healing for six cuts at the same severed location of an SRB 1.00 sample.

4. Conclusions

We have demonstrated an effective and simple approach to synthesize hybrid hydrogels with excellent resilience, super water-absorption ability, good conductivity, extremely fast electrical self-healing ability and excellent repeatable restoration of electrical performance and water-absorption ability. The commercial availability of the raw materials, easy fabrication and the excellent properties will help these versatile hydrogels to find more practical applications in soft moisture-related resistors/sensor systems.

Acknowledgments

Y. Tang is grateful for the research support of a Discovery Early Career Research Award (DECRA) from the Australian Research Council (Grant No.: DE120102784).

Reference

1. K. Kabiri, H. Omidian, M. J. Zohuriaan-Mehr and S. Doroudiani, *Polymer Composites*, 2011, **32**, 277-289.
2. M. Rani, A. Agarwal and Y. S. Negi, *BioResources*, 2010, **5**, 1-43.
3. M. Verhulsel, M. Vignes, S. Descroix, L. Malaquin, D. M. Vignjevic and J. L. Viovy, *Biomaterials*, 2014, **35**, 1816-1832.
4. K. Kabiri, H. Omidian, S. A. Hashemi and M. J. Zohuriaan-Mehr, *European*

Polymer Journal, 2003, **39**, 1341-1348.

5. S. Kiatkamjornwong, *ScienceAsia*, 2007, **33(s1)**, 039.
6. M. J. Zohuriaan-Mehr and K. Kabiri, *Iranian Polymer Journal (English Edition)*, 2008, **17**, 451-477.
7. F. L. Buchholz and A. T. Graham, eds., *Modern Superabsorbent Polymer Technology*, Wiley VCH, New York, 1998.
8. A. C. Estrada, A. L. Daniel-Da-Silva and T. Trindade, *RSC Advances*, 2013, **3**, 10828-10836.
9. H. Warren, R. D. Gately, P. O'Brien, R. Gorkin and M. I. H. Panhuis, *Journal of Polymer Science, Part B: Polymer Physics*, 2014.
10. J. Yang, C. R. Han, J. F. Duan, F. Xu and R. C. Sun, *ACS Applied Materials and Interfaces*, 2013, **5**, 3199-3207.
11. K. Haraguchi, *Polymer Journal*, 2011, **43**, 223-241.
12. C. W. Peak, J. J. Wilker and G. Schmidt, *Colloid and Polymer Science*, 2013, **291**, 2031-2047.
13. K. Zhang, M. A. Lackey, J. Cui and G. N. Tew, *Journal of the American Chemical Society*, 2011, **133**, 4140-4148.
14. Y. Okumura and K. Ito, *Advanced Materials*, 2001, **13**, 485-487.
15. J. P. Gong, Y. Katsuyama, T. Kurokawa and Y. Osada, *Advanced Materials*, 2003, **15**, 1155-1158.
16. M. A. Haque, T. Kurokawa and J. P. Gong, *Polymer*, 2012, **53**, 1805-1822.
17. K. Haraguchi and T. Takehisa, *Advanced Materials*, 2002, **14**, 1120-1124.
18. T. Nishida, H. Endo, N. Osaka, H. J. Li, K. Haraguchi and M. Shibayama, *Physical Review E - Statistical, Nonlinear, and Soft Matter Physics*, 2009, **80**.
19. P. Schexnailder and G. Schmidt, *Colloid and Polymer Science*, 2009, **287**, 1-11.
20. Q. Wang, J. L. Mynar, M. Yoshida, E. Lee, M. Lee, K. Okuro, K. Kinbara and T. Aida, *Nature*, 2010, **463**, 339-343.
21. B. C. K. Tee, C. Wang, R. Allen and Z. Bao, *Nature Nanotechnology*, 2012, **7**, 825-832.
22. S. Park and R. S. Ruoff, *Nature Nanotechnology*, 2009, **4**, 217-224.
23. V. C. Tung, M. J. Allen, Y. Yang and R. B. Kaner, *Nature Nanotechnology*, 2009,

4, 25-29.

24. A. Cao, Z. Liu, S. Chu, M. Wu, Z. Ye, Z. Cai, Y. Chang, S. Wang, Q. Gong and Y. Liu, *Advanced Materials*, 2010, **22**, 103-106.
25. N. I. Kovtyukhova, *Chemistry of Materials*, 1999, **11**, 771-778.
26. Y. K. Yang, C. E. He, W. J. He, L. J. Yu, R. G. Peng, X. L. Xie, X. B. Wang and Y. W. Mai, *Journal of Nanoparticle Research*, 2011, **13**, 5571-5581.
27. K. A. Mkhoyan, A. W. Contryman, J. Silcox, D. A. Stewart, G. Eda, C. Mattevi, S. Miller and M. Chhowalla, *Nano Letters*, 2009, **9**, 1058-1063.
28. Y. Yu, B. N. Murthy, J. G. Shapter, K. T. Constantopoulos, N. H. Voelcker and A. V. Ellis, *Journal of Hazardous Materials*, 2013, **260**, 330-338.
29. J. Lin, Q. Tang, J. Wu and S. Hao, *Reactive and Functional Polymers*, 2007, **67**, 275-281.
30. J. C. Meyer, A. K. Geim, M. I. Katsnelson, K. S. Novoselov, T. J. Booth and S. Roth, *Nature*, 2007, **446**, 60-63.
31. P. Huang, W. Chen and L. Yan, *Nanoscale*, 2013, **5**, 6034-6039.
32. Y. Lu, Y. Jiang, W. Wei, H. Wu, M. Liu, L. Niu and W. Chen, *Journal of Materials Chemistry*, 2012, **22**, 2929-2934.
33. H. J. Shin, K. K. Kim, A. Benayad, S. M. Yoon, H. K. Park, I. S. Jung, M. H. Jin, H. K. Jeong, J. M. Kim, J. Y. Choi and Y. H. Lee, *Advanced Functional Materials*, 2009, **19**, 1987-1992.